A&A 572, L10 (2014)
DOI: 10.1051/0004-6361/201424007

Astronomy & Astrophysics

Letter to the Editor

A non-equilibrium ortho-to-para ratio of water in the Orion PDR[⋆,⋆⋆]

Y. Choi[1,2], F. F. S. van der Tak[2,1], E. A. Bergin[3], and R. Plume[4]

[1] Kapteyn Astronomical Institute, University of Groningen, PO Box 800, 9700 AV Groningen, The Netherlands
e-mail: y.choi@astro.rug.nl
[2] SRON Netherlands Institute for Space Research, PO Box 800, 9700 AV Groningen, The Netherlands
[3] Department of Astronomy, University of Michigan, 500 Church Street, Ann Arbor, MI 48109, USA
[4] Department of Physics and Astronomy, University of Calgary, 2500 University Drive NW, Calgary, AB T2N 1N4, Canada

Received 16 April 2014 / Accepted 26 August 2014

ABSTRACT

Context. The ortho-to-para ratio (OPR) of H_2O is thought to be sensitive to the temperature of water formation. The OPR of H_2O is thus useful for studying the formation mechanism of water.
Aims. We investigate the OPR of water in the Orion PDR (photon-dominated region), at the Orion Bar and Orion S positions, using data from *Herschel*/HIFI.
Methods. We detect the ground-state lines of ortho- and para-$H_2^{18}O$ in the Orion Bar and Orion S and estimate the column densities using local thermodynamical equilibrium (LTE) and non-LTE methods.
Results. Based on our calculations, the OPR in the Orion Bar is 0.1−0.5, which is unexpectedly low given the gas temperature of ~85 K, and also lower than the values measured for other interstellar clouds and protoplanetary disks. Toward Orion S, our OPR estimate is below 2.
Conclusions. This low OPR at 2 positions in the Orion PDR is inconsistent with gas phase formation and with thermal evaporation from dust grains, but it may be explained by photodesorption.

Key words. ISM: molecules – ISM: individual objects: Orion Bar – ISM: individual objects: Orion S

1. Introduction

Water is an important reservoir of interstellar oxygen and therefore a key ingredient in the chemistry of oxygen-bearing molecules. In the interstellar medium (ISM), water can be formed by three different mechanisms. In cold molecular clouds, water may be formed in the gas phase by ion-molecule chemistry through dissociative recombination of H_3O^+. In cold and dense cores on the surfaces of cold dust grains, O and H atoms may combine to form water-rich ice mantles. These mantles will evaporate when the grains are heated to ~100 K by protostellar radiation or sputtered by outflow shocks. Third, in gas with temperatures above 300 K, reactions of O and OH with H_2 drive all gas-phase oxygen into water. Such high temperatures may occur very close to the star caused by heating of protostellar radiation or nearby outflow shocks (see van Dishoeck et al. 2013, for a review).

The hydrogen atom carries a nuclear spin angular momentum, and there are two species of molecular hydrogen (ortho-H_2 and para-H_2). Other molecules with two or more hydrogen atoms also exhibit this characteristic with two independent spin isomers (e.g., H_2O, NH_3, CH_4). Because of a difference in the energy of the rotational ground state (34 K for ortho-H_2O, 0 K for para-H_2O) the ratio of ortho-to-para water vapor depends on the gas temperature in thermal equilibrium. Above 40 K the ortho-to-para ratio (OPR) would be the ratio of the spin statistical weights of 3, and below this temperature there is an expectation that the formation of para-H_2O would be successively favored over ortho-H_2O, leading to a reduced OPR (Mumma et al. 1987). Since inelastic collisions do not change the OPR, this ratio may provide clues to the formation mechanism of water. The measured OPRs of H_2O is 2−3 in solar system comets (Mumma & Charnley 2011) and in Galactic interstellar clouds (Lis et al. 2013; Flagey et al. 2013), while an OPR of about one was measured for water vapor in the TW Hya disk (Hogerheijde et al. 2011).

In this paper we present measurements of the rotational emission of both spin isomers of water vapor toward the Orion photon-dominated region. Photon-dominated regions (PDRs) are the surface regions of molecular clouds, where ultraviolet radiation with photon energies between 6 and 13.6 eV drives the thermal and chemical balance of the gas (Hollenbach & Tielens 1999). Shielding of the UV radiation by dust and gas creates a layered structure where a sequence of different chemical transitions is produced by the gradual attenuation of the UV field (Ossenkopf et al. 2007).

The Orion Molecular Cloud 1 (OMC-1) is one of the nearest massive star-forming regions at a distance of ~420 pc (Menten et al. 2007). Parts of the OMC-1 region are ionized by the Trapezium cluster, creating an HII region. The Orion Bar PDR stands out as a ridge to the southeast of the Trapezium cluster. Observations at infrared and submillimeter wavelengths indicate a geometry for the Bar where the PDR is wrapped around the HII region created by the Trapezium stars changing it from a face-on to an edge-on view where the molecular emission peaks (Hogerheijde et al. 1995). The mean density of the Bar is about 10^5 cm^{-3}, and the gas temperature is 85 K in the interior, rising to ~150 K at the PDR surface (Larsson et al. 2003). The impinging radiation field is $(1{-}4) \times 10^4\ \chi_0$, where the Draine field

⋆ *Herschel* is an ESA space observatory with science instruments provided by European-led Principal Investigator consortia and with important participation from NASA.
⋆⋆ Appendices are available in electronic form at http://www.aanda.org

Table 1. Observed lines.

Source	Molecule	Transition	ν (GHz)	E_{up} (K)	T_{sys} (K)	t_{int} (min)	Beam (″)	η_{mb}	$\delta\upsilon$ (MHz)	rms (mK)
Orion Bar	o-$H_2{}^{18}O$	1_{10}–1_{01}	547.676	60.5	63	88	38.7	0.75	0.48	2.67
	p-$H_2{}^{18}O$	1_{11}–0_{00}	1101.698	53.4	350	56	19.2	0.74	1.1	102
Orion S	o-$H_2{}^{18}O$	1_{10}–1_{01}	547.676	60.5	71	7.4	38.7	0.75	1.1	26
	p-$H_2{}^{18}O$	1_{11}–0_{00}	1101.698	53.4	366	10	19.2	0.74	1.1	121

$\chi_0 = 2.7 \times 10^{-3}$ erg s^{-1} cm^{-2} (Draine 1978). The clumpiness of the PDR inferred by Hogerheijde et al. (1995) is confirmed by interferometric data (Lis & Schilke 2003), with densities of up to 1.5×10^6 to 6×10^6 cm^{-3}. In contrast, the densities of the interclump medium fall between a few 10^4 cm^{-3} (Young Owl et al. 2000) and 2×10^5 cm^{-3} (Simon et al. 1997).

Orion S is an active star-forming region, located 1′ southwest of the Trapezium, as indicated by the number of outflows and Herbig-Haro flows (Zapata et al. 2006). The mass of Orion S is ~100 $M_\odot$, and the size of this region is similar to that of Orion BN/KL, but its bolometric luminosity of 10^4 $L_\odot$ is an order of magnitude lower (Mezger et al. 1990), which may indicate that Orion S is less evolved (McMullin et al. 1993). The UV radiation field is estimated to be $\chi \sim 1.5 \times 10^5 \chi_0$ in Orion S (Herrmann et al. 1997), about a factor of 10 higher than that in the Orion Bar. The irradiation by the nearby Trapezium cluster means that the part of the Orion S region that faces the Trapezium cluster includes an ionization front and a face-on PDR.

This paper uses *Herschel*/HIFI observations of water lines in the Orion PDR, at the Orion Bar and Orion S positions. With its much higher spatial and spectral resolution and higher sensitivity than previous space missions, we investigate the OPR of water, providing new information on the formation mechanism of water in these regions.

2. Observations

The CO^+ peak in the Orion Bar was observed with the Heterodyne Instrument for the Far-Infrared (HIFI, de Graauw et al. 2010) onboard ESA's *Herschel* Space Observatory (Pilbratt et al. 2010) in all HIFI bands as part of the *Herschel* observations of EXtra-Ordinary Sources (HEXOS) guaranteed-time key program (Bergin et al. 2010). The coordinates of the observed position of the CO^+ peak in the Orion Bar are $05^h35^m20\overset{s}{.}6$ and −05°25′14″ (J2000).

In this paper we use the p-$H_2{}^{18}O$ 1_{11}−0_{00} line from the HIFI band 4b spectral line survey. This observation was carried out in April 2011 in load chop mode with a redundancy of 4 and with a total integration time of 0.7 h. The Wide-Band Spectrometer (WBS) backend was used, which covers 4 GHz bandwidth in four 1140 MHz subbands at 1.1 MHz resolution. In addition to the HIFI spectral scan, the o-$H_2{}^{18}O$ 1_{10}−1_{01} line was observed in September 2010 as a deep integration with a total integration time of 1.5 h in frequency switch mode.

Orion S was observed with a complete HIFI spectral scan as part of the HEXOS program. The observations were pointed toward $05^h35^m13\overset{s}{.}4$ and −05°24′08″1 (J2000). We used data from HIFI bands 1a (o-$H_2{}^{18}O$ 1_{10}−1_{01}) and 4b (p-$H_2{}^{18}O$ 1_{11}−0_{00}). The scans were observed using dual beam switch (DBS) observing mode. The WBS backend with a 1.1 MHz resolution was used.

We calibrated the data and removed standing waves and spurs, and did sideband deconvolution using the *Herschel* interactive processing environment (HIPE, Ott 2010) version 10.0. Further analysis was done by the CLASS[1] package.

The frequencies, energy of the upper levels, system temperatures, integration times, and rms noise level at a given spectral resolution for each of the lines are provided in Table 1, along with the beam sizes and main beam efficiencies from Roelfsema et al. (2012).

3. Results

The HIFI spectra of the Orion Bar show pure single-peaked emission profiles in the ground-state lines of para- and ortho-$H_2{}^{18}O$ (Fig. A.1). In contrast, in Orion S, the ground-state line of ortho-$H_2{}^{18}O$ appears in emission, but the ground-state line of para-$H_2{}^{18}O$ is detected in absorption (Fig. A.2). This effect may be due to the stronger continuum in Orion S than in the Orion Bar, which increases toward higher frequencies, assuming the dust and gas are well mixed (continuum level ~4.6 K at 1101.7 GHz in Orion S compared to 0.3 K for the Bar). In addition, LVG models by Cernicharo et al. (2006) predict that ortho- and para-H_2O lines appear in absorption or emission depending on the adopted conditions.

We extract line parameters from the observed profiles by fitting Gaussians. The o-$H_2{}^{18}O$ 1_{10}−1_{01} in Orion S has a hint of a self-reversal, but this is unfortunately at the level of noise in the data, and the parameters of this line were determined by fitting one Gaussian; Table 2 gives the results for all lines. The components in the Orion Bar show similar line profiles, $\Delta V \sim 1.8$–1.9 km s^{-1} and $V_{LSR} \sim 10$ km s^{-1}, suggesting that these two lines originate in the same gas. These parameters are also similar to those of CO, H_2CO, and other dense gas tracers (Leurini et al. 2006). On the other hand, the line profiles in Orion S have a width of 4.6–5.5, which is broader than in the Orion Bar, and a velocity of ~7.0–7.4 km s^{-1}. This velocity shift is commensurate with the known N-S velocity gradient seen along the Orion Molecular Ridge (Ungerechts et al. 1997). The observed line widths and LSR velocities are similar to those of CO isotopologues (Peng et al. 2012).

4. Analysis

4.1. Orion Bar

We estimate column densities assuming LTE and also explored models where the populations are not in LTE. For the LTE calculations, we have some additional supporting evidence based on other observations of both sources obtained as part of the HEXOS program. (1) The ground-state lines of $H_2{}^{17}O$ are not detected (rms ~ 0.04 K at the o-$H_2{}^{17}O$ 1_{10}−1_{01} line and rms ~ 0.2 K at the p-$H_2{}^{17}O$ 1_{11}−0_{00} line), which limits the optical depth of the $H_2^{18}O$ lines to be below 0.7. In the following we assume that the emission is optically thin. (2) The water emission does not arise from very warm (>100 K) and dense gas (>10^8 cm^{-3}) toward either the Orion Bar or Orion S because

[1] http://www.iram.fr/IRAMFR/GILDAS/

Table 2. Line parameters obtained from Gaussian fits.

Source	Molecule	Transition	$\int T_{\rm MB} {\rm d}V$ (K km s^{-1})	$V_{\rm LSR}$ (km s^{-1})	ΔV (km s^{-1})	$T_{\rm MB}$ (K)
Orion Bar	o-$H_2{}^{18}O$	1_{10}–1_{01}	0.23 (0.01)	10.22 (0.01)	1.93 (0.03)	0.11
	p-$H_2{}^{18}O$	1_{11}–0_{00}	0.56 (0.12)	9.91 (0.19)	1.84 (0.48)	0.29
Orion S	o-$H_2{}^{18}O$	1_{10}–1_{01}	1.17 (0.06)	7.45 (0.13)	4.66 (0.27)	0.23
	p-$H_2{}^{18}O$	1_{11}–0_{00}	3.48 (0.27)	7.05 (0.18)	5.53 (0.64)	–0.59[a]

Notes. [(a)] Absorption line detected in Orion S.

we do not detect emission arising from excited states (p-$H_2^{18}O$ 2_{02}–1_{11}, o-$H_2{}^{18}O$ 2_{12}–1_{01}, rms ~ 0.2–0.7 K), which implies a limit on the excitation temperature of less than 100 K. (3) The difference in beam size between the ortho-$H_2{}^{18}O$ 547 GHz line and para-$H_2{}^{18}O$ 1101 GHz line observations could lead us to underestimate the OPR by factors up to 4. However, this is unlikely since water emission in the Orion ridge extends over several arcminutes (Melnick et al. 2011). Furthermore, the detected lines are likely to come from the same gas when considering the velocities and line widths (see Table 2).

We therefore derive the column densities of ortho- and para-$H_2^{18}O$ in the Orion Bar for different excitation temperatures ($T_{\rm ex}$ = 50–100 K) and find values of ~3.0×10^{10} cm^{-2} for the ortho-$H_2^{18}O$ line and ~1.0×10^{11} cm^{-2} for the para-$H_2^{18}O$ line. The derived column densities are not strongly sensitive to the assumed excitation temperature. With the above assumptions, and in LTE, we derive an OPR of ~0.3.

The ground-state emission lines of ortho- and para-water are not identical in their excitation characteristics. Moreover, both lines have high critical densities so we explore non-LTE models of H_2O using the RADEX code (van der Tak et al. 2007) and state-of-the-art quantum mechanical collision rates of para- and ortho-H_2O with para- and ortho-H_2 (Daniel et al. 2011) as provided at the LAMDA database (Schöier et al. 2005), assuming thermal values for the o/p ratio of H_2. For this exploration we generate a grid of models with values of $T_{\rm kin}$ = 20, 60, and 100 K and values of $n(H_2) = 10^4$, 10^6, and 10^8 cm^{-3}, and fix the background radiation temperature at 2.73 K for the Orion Bar. Within the range of assumed densities and temperatures we find that the analysis remains consistent with a low OPR with values ranging from 0.1 to 0.5 (see Table B.1). For the case where H_2O emission is arising from the warm surface of the PDR (e.g. Hollenbach et al. 2009), we present an additional solution with $T_{\rm gas}$ = 200 K. For the density we use the detailed model of Nagy et al. (2013), which has a density of 10^5 cm^{-3} at 200 K, and with this assumption the derived OPR is 0.14.

As an alternative background radiation field, we adopt a modified blackbody distribution with a dust temperature of $T_{\rm d}$ = 49 K and a dust emissivity index of β = 1.6 for the interior of the Orion Bar (Arab et al. 2012), so that the absolute dust opacity of $\tau_{\rm d}$ = 0.21 at 971 GHz. This model predicts that the column densities are similar to those at the background radiation temperature of 2.73 K under the same conditions of $T_{\rm kin}$ and $n(H_2)$, and the OPR of water is ~0.1–0.5 (Table B.1).

4.2. Orion S

To estimate the column density for the absorption component of p-$H_2{}^{18}O$ 1_{11}–0_{00}, which is detected in Orion S, we derive the optical depth using the expression

$$\tau = -\ln\left(\frac{T_{\rm line}}{T_{\rm cont}}\right) \tag{1}$$

where $T_{\rm cont}$ is the single side band (SSB) continuum intensity assuming that the continuum is completely covered by the absorbing layer and $T_{\rm line}$ is the intensity at the absorption dip with continuum. We apply a linear baseline fit in the vicinity of the absorption line to derive the continuum intensity (~4.6 K with uniform beam filling) at the absorption peak. Deriving the optical depth from the line-to-continuum ratio is based on the assumption that the excitation temperature is negligible with respect to the continuum temperature (i.e., no emission filling in the absorption) and that the line is not saturated.

If all water molecules are in the para ground state, the velocity integrated absorption is related to the molecular column density by

$$N = \frac{8\pi\nu^3 g_{\rm l}}{c^3 A g_{\rm u}} \int \tau {\rm d}V, \tag{2}$$

where N is the column density, ν the frequency, c the speed of light, and τ is the optical depth. Here, A stands for the Einstein-A coefficient, and $g_{\rm l}$ and $g_{\rm u}$ are the degeneracy of the lower and the upper level of the transition. Integrating between $V = 0$ and 13 km s^{-1}, we find a column density of ~2.0×10^{12} cm^{-2} for the para-$H_2^{18}O$ line in Orion S.

Assuming LTE and using the same assumptions as for the Bar, given the limit on the optical depth (<0.7) by the non-detection of $H_2^{17}O$ and the $T_{\rm ex}$ limit (<100 K) from the excited states, we find a beam-averaged column density of ~2.0×10^{11} cm^{-2} for the ortho-$H_2^{18}O$ line. Thus, assuming LTE, the OPR of water is ~0.1 in Orion S.

As before we perform a series of non-LTE calculations to confirm the low OPR derived for Orion S assuming LTE. We therefore generate a grid of models with values of $T_{\rm kin}$ and $n(H_2)$, and a background radiation field of 2.73 K. We find an OPR ~ 0.3 assuming $T_{\rm kin}$ = 100 K and $n(H_2) = 10^8$ cm^{-3}, but derive a value of 3 (or unphysically higher than 3) if $T_{\rm kin}$ = 60 K and $n(H_2) = 10^6$ cm^{-3} or for $T_{\rm kin}$ = 20 K and $n(H_2) = 10^4$ cm^{-3}. Thus the derived OPR of water is strongly sensitive to the assumed physical conditions (Table B.1).

Further constraints on the OPR in Orion S come from the non-detection of the ortho-$H_2{}^{18}O$ 2_{12}–1_{01} line (1655.9 GHz) in our survey. This line connects to the ortho-H_2O ground state and arises at a much higher frequency where the continuum level is higher (~6.1 K) than at the frequency of the para-H_2O ground-state line. This non-detection of the ortho-$H_2{}^{18}O$ 2_{12}–1_{01} line in either emission or absorption gives information on the limit of the ortho-H_2O column density in the absorbing gas. Assuming that the ground-state line of ortho-$H_2{}^{18}O$ 2_{12}–1_{01} appears in absorption, we estimate its optical depth. We adopt a line width of 5.5 km s^{-1} from the para-$H_2{}^{18}O$ 1_{11}–0_{00} line observations, a continuum intensity of 6.1 K, and an rms of 0.4 K from the ortho-$H_2{}^{18}O$ 2_{12}–1_{01} line observations. Assuming that the OPRs of water are 3, 2.5, 2, and 1, we derive a $T_{\rm line}$ of 4.8, 5.0, 5.2, and 5.6 K, respectively, using Eqs. (1) and (2). If the OPRs of water are 3 and 2.5, we should see absorption lines of ortho-$H_2{}^{18}O$ $2_{12}-1_{01}$ with optical depth of 0.24 and 0.20, respectively. However, for OPRs of 1 and 2, the ortho-$H_2{}^{18}O$ $2_{12}-1_{01}$ would be seen in absorption with optical depth of 0.16 and 0.08 (within the noise), as illustrated in Fig. C.1. We conclude that our data are consistent with OPR $\leq$ 2 for cold water, but not with OPR $\geq$ 2.5.

5. Discussion

Our derived OPR of H_2O in the Orion Bar is 0.1−0.5 (T_{spin} ~ 8−12 K), which is well below in other ISM sources and even lower than toward TW Hya. It is also much lower than expected based on the gas temperature of ~85 K (Hogerheijde et al. 1995). Furthermore, the OPR of water in Orion S is below 2 (T_{spin} < 23 K).

Currently it is uncertain how low OPRs originate. Gas phase formation via H_3O^+ dissociative recombination is expected to lead to an OPR of 3 because the reaction is exothermic, and the energy releases exceeds the ortho/para energy difference (Hogerheijde et al. 2011). It cannot originate in grain surfaces due to thermal evaporation because the measured dust temperature toward the Bar (and presumably Orion S) is ~35−70 K (Arab et al. 2012), which is below the evaporation temperature of water ice (~100 K; Fraser et al. 2001)

The low water OPR may be explained by photodesorption, which has been argued to be the main formation mechanism for cold water vapor in the dense ISM (Hollenbach et al. 2009). In addition, a direct observational proof for photodesorption of H_2O is provided by the detection of gas-phase H_2O toward the pre-stellar core L1544 (Caselli et al. 2012) and NGC 1333-IRAS4A protostar (Mottram et al. 2013). There are two possible processes for photodesorption, following photodissociation of H_2O ice into H and OH after absorption of a UV photon (Andersson & van Dishoeck 2008; Arasa et al. 2010; Tielens 2013; van Dishoeck et al. 2013): 1) H and OH recombine in the ice to form H_2O, which then has sufficient energy to desorb; 2) the energetic H atom kicks out a neighboring H_2O molecule from the ice, which is initiated by the same UV photon. In Option 1, the OPR should go to the statistical value of 3 because of the exothermicity of the reaction. In Option 2, the original OPR in the ice should be preserved. If the grain temperature is low and the OPR equilibrated to the grain temperature, the OPR should be low, in agreement with our results. The relative importance of Options 1 and 2 depends on the thickness of the ice layer and to a lesser extent on the ice temperature. Roughly, they contribute about equally, but a detailed calculation is beyond the scope of this work. The experiments by Yabushita et al. (2009) show that the measured translational and rotational energies of H_2O (v = 0) molecules photodesorbed from amorphous solid water are in good agreement with those predicted by classical molecular dynamics calculations for the "kick-out" mechanism (Option 2).

The OPRs of water have been measured in many different environments, but the *Herschel*/HIFI H_2O observations in the Orion PDR show an unusually low OPR of water. This opportunity will be further explored in a future paper, where we will estimate OPR of other molecules in the Orion PDR and will compare OPR of water in other PDRs. In addition, the *Herschel*/HIFI H_2O observations toward the Orion PDR show the structure in more detail than any previous study. It will also be further studied in a future paper, where we will estimate H_2O abundance profiles.

Acknowledgements. We thank the referee for the constructive suggestions. We also thank the editor, Malcolm Walmsley, for additional helpful comments. The authors thank Ewine van Dishoeck, Edith Fayolle, Jean-Hugh Fillion, and Annemieke Petrignani for useful discussions on photodesorption. HIFI has been designed and built by a consortium of institutes and university departments from across Europe, Canada, and the US under the leadership of SRON Netherlands Institute for Space Research, Groningen, The Netherlands, with major contributions from Germany, France and the US. Consortium members are: Canada: CSA, U.Waterloo; France: CESR, LAB, LERMA, IRAM; Germany: KOSMA, MPIfR, MPS; Ireland, NUI Maynooth; Italy: ASI, IFSI-INAF, Arcetri-INAF; Netherlands: SRON, TUD; Poland: CAMK, CBK; Spain: Observatorio Astronómico Nacional (IGN), Centro de Astrobiología (CSIC-INTA); Sweden: Chalmers University of Technology MC2, RSS & GARD, Onsala Space Observatory, Swedish National Space Board, Stockholm University Stockholm Observatory; Switzerland: ETH Zürich, FHNW; USA: Caltech, JPL, NHSC.

References

Andersson, S., & van Dishoeck, E. F. 2008, A&A, 491, 907
Arab, H., Abergel, A., Habart, E., et al. 2012, A&A, 541, A19
Arasa, C., Andersson, S., Cuppen, H. M., van Dishoeck, E. F., & Kroes, G.-J. 2010, J. Chem. Phys., 132, 184510
Bergin, E. A., Phillips, T. G., Comito, C., et al. 2010, A&A, 521, L20
Caselli, P., Keto, E., Bergin, E. A., et al. 2012, ApJ, 759, L37
Cernicharo, J., Goicoechea, J. R., Pardo, J. R., & Asensio-Ramos, A. 2006, ApJ, 642, 940
Daniel, F., Dubernet, M.-L., & Grosjean, A. 2011, A&A, 536, A76
de Graauw, T., Helmich, F. P., Phillips, T. G., et al. 2010, A&A, 518, L6
Draine, B. T. 1978, ApJS, 36, 595
Flagey, N., Goldsmith, P. F., Lis, D. C., et al. 2013, ApJ, 762, 11
Fraser, H. J., Collings, M. P., McCoustra, M. R. S., & Williams, D. A. 2001, MNRAS, 327, 1165
Herrmann, F., Madden, S. C., Nikola, T., et al. 1997, ApJ, 481, 343
Hogerheijde, M. R., Jansen, D. J., & van Dishoeck, E. F. 1995, A&A, 294, 792
Hogerheijde, M. R., Bergin, E. A., Brinch, C., et al. 2011, Science, 334, 338
Hollenbach, D. J., & Tielens, A. G. G. M. 1999, Rev. Mod. Phys., 71, 173
Hollenbach, D., Kaufman, M. J., Bergin, E. A., & Melnick, G. J. 2009, ApJ, 690, 1497
Larsson, B., Liseau, R., Bergman, P., et al. 2003, A&A, 402, L69
Leurini, S., Rolffs, R., Thorwirth, S., et al. 2006, A&A, 454, L47
Lis, D. C., & Schilke, P. 2003, ApJ, 597, L145
Lis, D. C., Bergin, E. A., Schilke, P., & van Dishoeck, E. F. 2013, J. Phys. Chem. A, 117, 9661
McMullin, J. P., Mundy, L. G., & Blake, G. A. 1993, ApJ, 405, 599
Melnick, G. J., Tolls, V., Snell, R. L., et al. 2011, ApJ, 727, 13
Menten, K. M., Reid, M. J., Forbrich, J., & Brunthaler, A. 2007, A&A, 474, 515
Mezger, P. G., Zylka, R., & Wink, J. E. 1990, A&A, 228, 95
Mottram, J. C., van Dishoeck, E. F., Schmalzl, M., et al. 2013, A&A, 558, A126
Mumma, M. J., & Charnley, S. B. 2011, ARA&A, 49, 471
Mumma, M. J., Weaver, H. A., & Larson, H. P. 1987, A&A, 187, 419
Nagy, Z., Van der Tak, F. F. S., Ossenkopf, V., et al. 2013, A&A, 550, A96
Ossenkopf, V., Rollig, M., Cubick, M., & Stutzki, J. 2007, in Molecules in Space and Laboratory, meeting held in Paris, 95
Ott, S. 2010, in Astronomical Data Analysis Software and Systems XIX, eds. Y. Mizumoto, K.-I. Morita, & M. Ohishi, ASP Conf. Ser., 434, 139
Peng, T.-C., Wyrowski, F., Zapata, L. A., Güsten, R., & Menten, K. M. 2012, A&A, 538, A12
Pilbratt, G. L., Riedinger, J. R., Passvogel, T., et al. 2010, A&A, 518, L1
Roelfsema, P. R., Helmich, F. P., Teyssier, D., et al. 2012, A&A, 537, A17
Schöier, F. L., van der Tak, F. F. S., van Dishoeck, E. F., & Black, J. H. 2005, A&A, 432, 369
Simon, R., Stutzki, J., Sternberg, A., & Winnewisser, G. 1997, A&A, 327, L9
Tielens, A. G. G. M. 2013, Rev. Mod. Phys., 85, 1021
Ungerechts, H., Bergin, E. A., Goldsmith, P. F., et al. 1997, ApJ, 482, 245
van der Tak, F. F. S., Black, J. H., Schöier, F. L., Jansen, D. J., & van Dishoeck, E. F. 2007, A&A, 468, 627
van Dishoeck, E. F., Herbst, E., & Neufeld, D. A. 2013, Chem. Rev., 113, 9043
Yabushita, A., Hama, T., Yokoyama, M., et al. 2009, ApJ, 699, L80
Young Owl, R. C., Meixner, M. M., Wolfire, M., Tielens, A. G. G. M., & Tauber, J. 2000, ApJ, 540, 886
Zapata, L. A., Ho, P. T. P., Rodríguez, L. F., et al. 2006, ApJ, 653, 398

Pages 5 to 6 are available in the electronic edition of the journal at http://www.aanda.org

Appendix A: Spectra of the ground-state $H_2^{18}O$ lines

In Sect. 3, we present the ground-state lines of ortho- and para-$H_2^{18}O$ observed with *Herschel*/HIFI toward the Orion Bar (Fig. A.1) and Orion S (Fig. A.2).

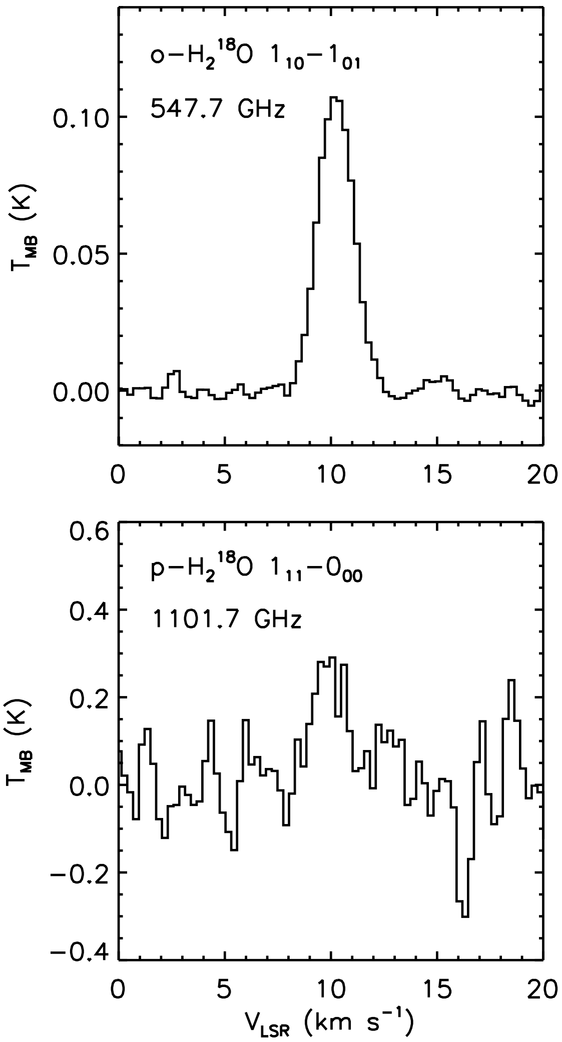

Fig. A.1. Spectra of the ground-state $H_2^{18}O$ lines in the Orion Bar. The weak continuum has been subtracted.

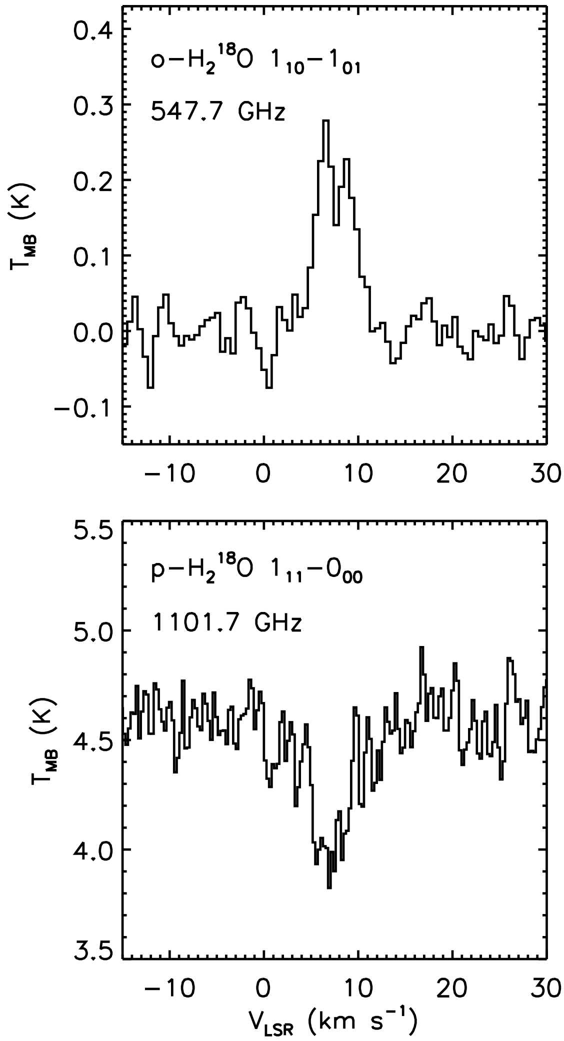

Fig. A.2. Spectra of the ground-state $H_2^{18}O$ lines toward Orion S. For the o-$H_2^{18}O$ line, the continuum has been subtracted. The p-$H_2^{18}O$ line shows absorption against the continuum.

Table B.1. Examples of column densities for the adopted conditions from a full grid non-LTE calculations in the Orion Bar and Orion S.

Source	Molecule	Transition	$T_{\rm kin}$ and $n(H_2)$ (K and cm^{-3}) 20 and 10^4	60 and 10^6	100 and 10^8
			N from RADEX Model with $T_{\rm bg}$ = 2.73 K (cm^{-2})		
Orion Bar	o-$H_2{}^{18}O$	1_{10}–1_{01}	2.19×10^{15}	1.65×10^{12}	1.20×10^{11}
	p-$H_2{}^{18}O$	1_{11}–0_{00}	3.08×10^{16}	1.75×10^{13}	2.66×10^{11}
Orion S	o-$H_2{}^{18}O$	1_{10}–1_{01}	1.13×10^{16}	8.57×10^{12}	6.06×10^{11}
			N from RADEX Model with T_d = 49 K and β = 1.6 (cm^{-2})		
Orion Bar	o-$H_2{}^{18}O$	1_{10}–1_{01}	–	2.80×10^{12}	1.49×10^{11}
	p-$H_2{}^{18}O$	1_{11}–0_{00}	–	2.01×10^{13}	2.96×10^{11}

Appendix B: Column densities derived by non-LTE RADEX code

In Sect. 4, for the non-LTE calculations of ortho- and para-$H_2{}^{18}O$ lines, we generate a grid of models with values of $T_{\rm kin}$ = 20, 60, and 100 K and values of $n(H_2) = 10^4$, 10^6, and 10^8 cm^{-3}, and fix the background radiation temperature at 2.73 K for the Orion Bar and Orion S using the RADEX code (van der Tak et al. 2007). Table B.1 presents the derived column densities for the adopted conditions from a full grid non-LTE calculations as examples. The p-$H_2^{18}O$ 1_{11}–0_{00} line in Orion S appears in absorption so we derive the column density using the optical depth (see Sect. 4.2 for details).

As an additional model for the Orion Bar, for the background radiation field we adopt a modified blackbody distribution with a dust temperature of T_d = 49 K and a dust emissivity index of β = 1.6 by Arab et al. (2012) for the interior of the Orion Bar, so that the absolute dust opacity of τ_d = 0.21 at 971 GHz. This RADEX model shows that ortho- and para-$H_2^{18}O$ lines appear in absorption at low density and low temperature (at $T_{\rm kin}$ = 20 K & $n(H_2) = 10^4$ cm^{-3}), which is not consistent with our observations.

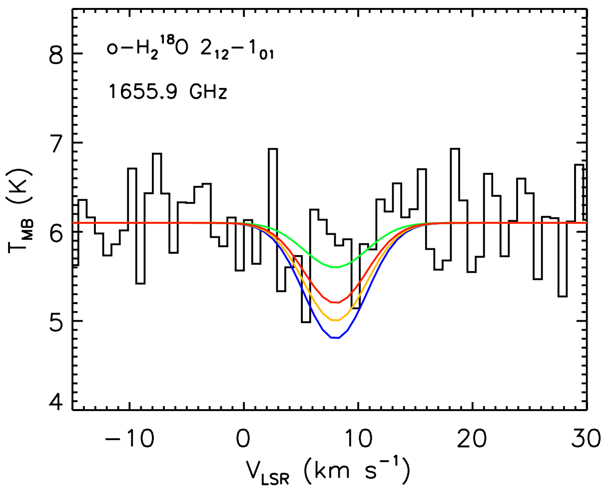

Fig. C.1. Four absorption lines on top of spectra of the ground-state ortho-$H_2^{18}O$ 2_{12}–1_{01} line (black), with continuum in Orion S. Assuming that the OPRs are 1, 2, 2.5, and 3, the derived optical depth of 0.08, 0.16, 0.20, and 0.24 are presented, respectively, as green, red, yellow, and blue.

Appendix C: Further constraints on the OPR in Orion S

In Sect. 4.2, we estimate the intensity of the ground-state line of ortho-$H_2{}^{18}O$ 2_{12}–1_{01} (1655.9 GHz) assuming that this line appears in absorption to constrain the OPR in Orion S. In Fig. C.1 we present four absorption lines on top of the ground-state ortho-$H_2{}^{18}O$ 2_{12}–1_{01} line. The green, red, yellow, and blue lines represent absorption lines with optical depth of 0.08, 0.16, 0.20, and 0.24, respectively.